The Journal of Engineering

The 9th International Conference on Power Electronics, Machines and Drives (PEMD 2018)

IET Journals
The Institution of Engineering and Technology

Bidirectional marx DC–DC converter for offshore wind farm application

eISSN 2051-3305
Received on 25th June 2018
Accepted on 31st July 2018
E-First on 14th May 2019
doi: 10.1049/joe.2018.8222
www.ietdl.org

Samir Milad Alagab[1] ✉, *Sarath Tennakoon*[1], *Chris Gould*[1]

[1]*School of Creative Arts and Engineering, Staffordshire University, Stoke on Trent, United Kingdom*

✉ *E-mail: Samir.alagab@research.staffs.ac.uk*

Abstract: The bidirectional DC–DC converter explained here is based on the Marx principle and is capable of achieving step-up and step-down voltage transformations at kV level and is able to handle MW-level power transfers in both directions. The main features of this topology are the absence of a high-frequency transformer, reduced weight, volume, and soft switching to reduce the switching losses. In the boost mode, five capacitors are charged in parallel and discharged in series to achieve the step-up action, and in the buck mode, the converse action takes place. The operating principle is explained, and the steady-state analysis of the converter is given. Matlab/Simulink simulation of a 50 MW converter, interfacing 6 kV, and 30 kV systems supports and validates the theoretical analysis, enables positive supporting the conclusions to be made.

1 Introduction

A high-voltage direct current (HVDC) grid is a natural extension of the grid integration of large offshore wind farms using voltage source converter (VSC)-based HVDC systems. Such systems would require the interconnection of sections operating at different DC-voltage levels through DC–DC converters [1]. The power flow through the DC–DC converter needs to be in both directions. During normal generation, the power flow is from the wind farm to the grid. However, when the wind farm is not generating, the auxiliaries in the wind farm require a small amount of power which must be drawn from the grid. Therefore, the DC–DC converter needs to be bidirectional.

This paper is organised as follows: in Section 2, a number of bidirectional DC–DC converter topologies found in literature are explained. A new bidirectional converter and its steady-state analysis is presented in Sections 3 and 4, respectively. In Section 5, a simulation study in the forward and reverse mode has been presented. Finally, conclusions are drawn in Section 6.

2 Bidirectional DC–DC converter topologies

Dual active bridge (DAB) converter [2–5] shown in Fig. 1*a* typically operates at a high switching frequency in order to reduce the size of the transformer. Although these topologies use soft switching to reduce switching losses, their magnetic core losses are still high and have high ripple currents and large leakage inductances. These converters also require complex control.

Thomas [5] has presented three types of DAB converter, which require complex control. Xing [6] presented a modular bidirectional buck/boost DC/DC converter for HVDC grid as illustrated in Fig. 1*b*. It uses small sub-module capacitors when compared to the modular multilevel converter, which will significantly reduce the converter volume and weight, but the drawback of this converter is the variable duty cycle and large inductance.

In Fig. 1*c*, Pires [7] presented a bi-directional buck/boost converter for electrochemical storage devices. The voltage ratio of this converter is high, but has a variable duty cycle in both forward and reverse operation. The switching frequency is high, leading to high switching losses and hence is impractical in high power converters.

Dragan [8] proposed a high-power DC converter without a transformer which uses thyristors as switching devices as shown in Fig. 1*d*. It can transfer the power in both directions and has an ability to isolate faults. However, the Dragan's converter has eight inductors and requires several switches in series to withstand the high voltage.

LCL bidirectional DC–DC converter [9, 10] shown in Fig. 1*e* uses IGBTs unlike the Dragan converter [8]. The advantage of this converter is the ability to achieve current regulation, even under extreme external DC faults and soft switching to reduce the switching losses. The disadvantage of this converter is the large size of inductor requires to reduce the current ripple and requires series connection of devices. In addition, Kolparambath presented

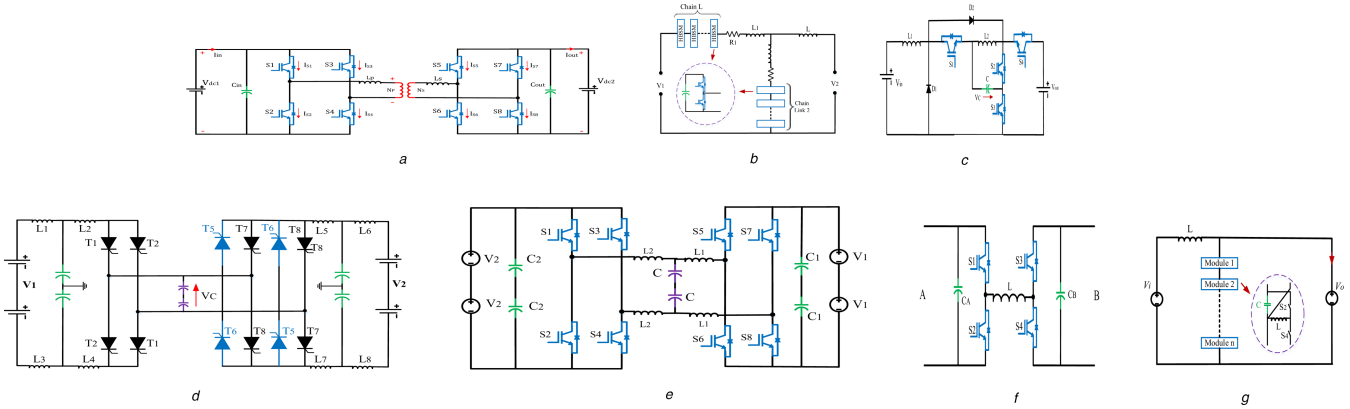

Fig. 1 *Common bidirectional DC-DC converter topologies*
(a) DAB, ***(b)*** Modular buck/boost, ***(c)*** buck/boost quadratic, ***(d)*** Thyristor converter, ***(e)*** IGBT converter, ***(f)*** Four quadrant converter, and ***(g)*** MMC converter

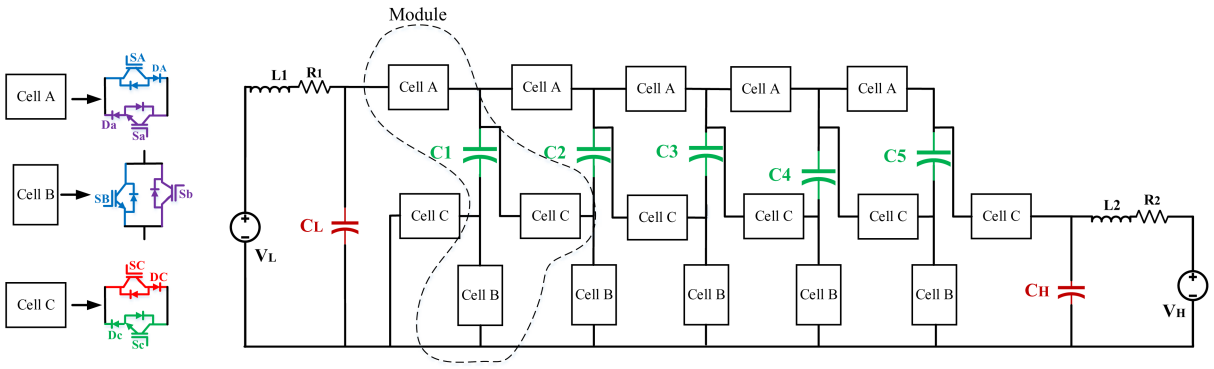

Fig. 2 *Bidirectional DC-DC converter*

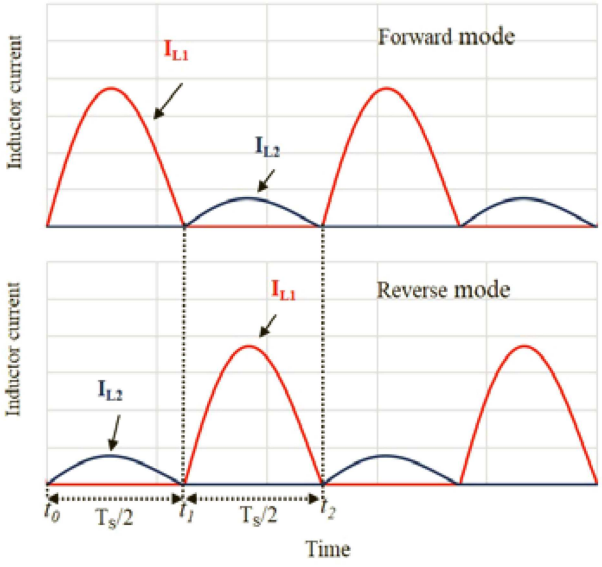

Fig. 3 *Inductor current waveforms during both modes*

an LCL bidirectional DC–DC converter in multi-terminal direct-current MTDC systems [11] as depicted in Fig. 1*f*. This converter has one inductor which is an advantage, high-voltage ratio, and a low switching frequency. However, the inductor is large and requires many switches in series to withstand the high voltage. This converter uses hard switching, which leads to high switching losses.

Filsoof [12] developed a bidirectional modular multilevel DC–DC converter of the triangular structure as illustrated in Fig. 1*g*. This converter has a significant reduction in the output voltage ripple and input current. However, this topology suffers from high switching frequency and has a two-level structure with only one boost inductor. This leads to design difficulties for HVDC application.

3 Bidirectional DC–DC marx converter

3.1 Circuit configuration

The main circuit of the bidirectional DC–DC Marx converter is illustrated in Fig. 2. It consists of three circuits. The first circuit is comprised of inductor L_1 and capacitor C_L connected in series with DC voltage V_L.

There are five identical modules in the second circuit. Each module is composed of three cells: A, B, and C; cells A and C have two anti-parallel IGBT switches with diodes connected in series and a capacitor for holding the cell voltage. Cell B has two anti-parallel IGBT switches only. The converter can transfer the power in both directions and scale the voltage up or down the transformation ratio by changing the number of modules. The third circuit is similar to the first consisting of the inductor L_2 and the capacitor C_H connected in series with the DC voltage V_H

3.2 Operating principle

The operation of the converter is based on the Marx generator concept. Five modules are used to achieve a voltage ratio of 1:5. In this study, a range of power levels up to 50 MW in the forward direction and up to 5 MW in reverse direction are considered.

All the IGBTs are switched at zero current to reduce the switching losses. In addition, all the switches must be capable of bidirectional blocking and forward conducting. The converter operation can be divided into two modes of operation: forward mode (FM) and reverse mode (RM).

3.2.1 Forward mode: In this mode, the energy flows from the low-voltage side to the high-voltage side. FM can also be divided into two sub-commutations. In the first sub-commutation (t_0–t_1) as shown in Fig. 3, the charging current flows through five capacitors (C_1–C_5) in parallel by switching ON switches (S_A–S_B), while all the other switches are turned OFF, as shown in Fig. 4. The diodes (D_A) block the reverse current flow.

In the second sub-commutation (t_1–t_2), the capacitors that were charged during the first sub-commutation are discharged in series to create the high voltage on the HV side by switching ON switches (SC), while diodes (DC) block the reverse current flow during capacitor discharge.

In this case, as there are five modules and the voltage gain is 5 and the electric charges is transferred from the five series-connected capacitors C_1, C_2, C_3, C_4 and C_5 to the capacitor C_H as depicted in Fig. 5.

3.2.2 Reverse mode: As shown in Fig. 6, the current flows from high-voltage V_H to the low-voltage V_L. In the first sub-commutation, inductor current I_{L2} charges the five capacitors (C_1–

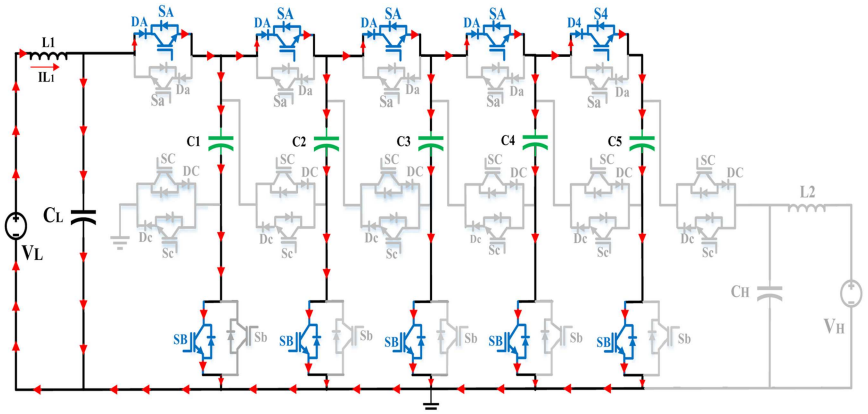

Fig. 4 *Switching and corresponding current flow directions of charging capacitors in parallel in forward mode*

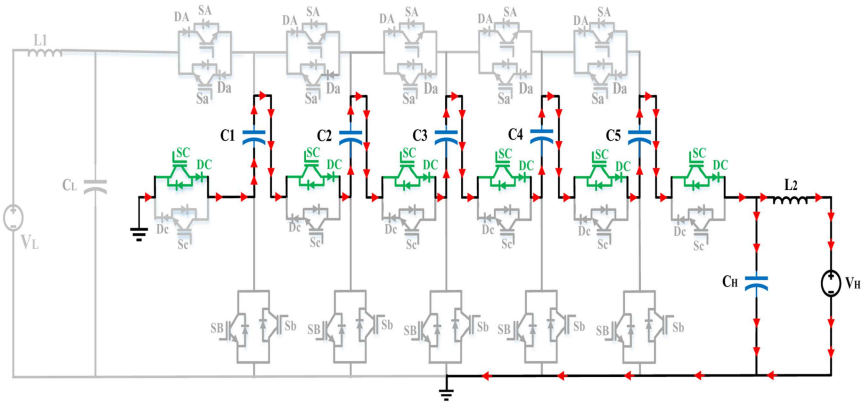

Fig. 5 *Switching and corresponding current flow directions of discharging capacitors in series in FM*

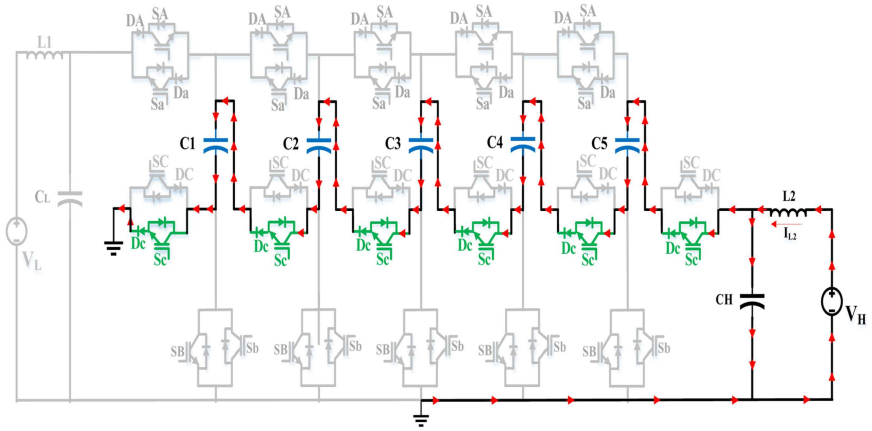

Fig. 6 *Switching and corresponding current flow direction of charging capacitors in series in reverse mode*

C_5) in series in time interval (t_0–t_1), as shown in Fig. 3, by switching ON switches (S_C) and diodes (D_C), are connected in series with switches (S_C) to ensure unidirectional transfer of charge from the voltage source VH, to series-connected capacitors and which are forward biased, while all the other switches are turned OFF.

In the second sub-commutation, the switches (S_a, S_b) are turned ON, and the capacitors are discharged in parallel in time interval (t_1–t_2) to the low-voltage V_L through inductor L_1 as depicted in Fig. 3, while the other switches are turned OFF as shown in Fig. 7.

4 Steady-state analysis

It is assumed that the converter has reached the steady-state condition. The converter voltage gain is the same as the number of capacitors 'n' and hence

$$n = \frac{V_H}{V_L} \tag{1}$$

where V_L and V_H are the low side and high side voltages, respectively. The equivalent capacitance in forward mode at the first sub-commutation is

$$C_{eq} = \sum_{k=1}^{k} C_i \tag{2}$$

where C_i is the capacitance, and C_{eq} is the equivalent capacitance of parallel connected capacitors in the first sub- commutation. However, in the first-commutation, the inductor L_1 and the equivalent capacitance $C_{eq\,(J)}$ forms an oscillatory L–C circuit and hence the current in the first sub-commutation is given by

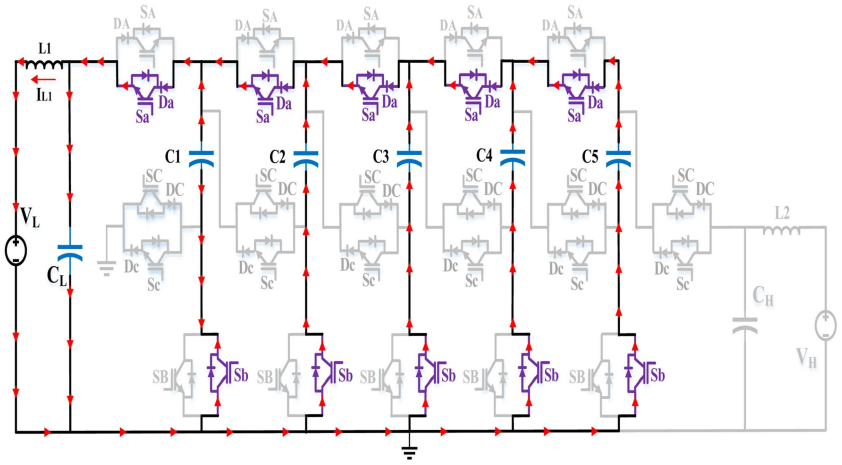

Fig. 7 *Discharging capacitors in parallel in reverse mode*

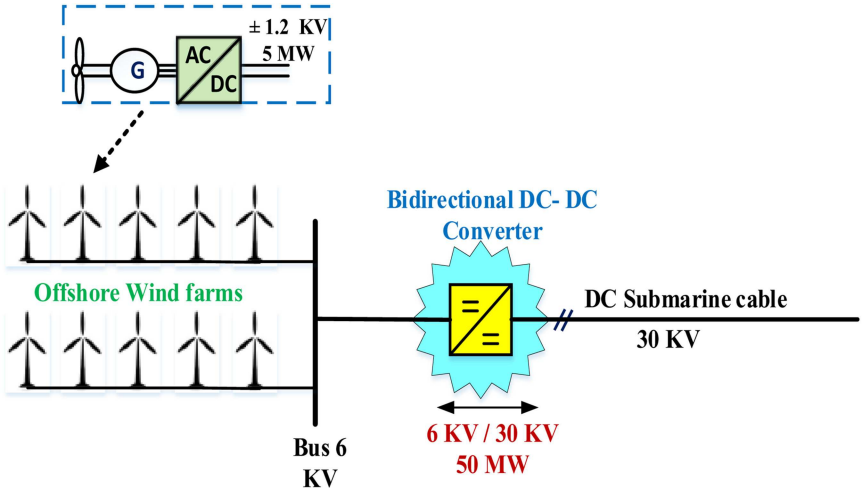

Fig. 8 *DC collection topology system of wind farm*

$$i_{L1} = i_{ceq} = \frac{V_L}{\omega L_1}\sin(\omega t) \tag{3}$$

and

$$\omega = \frac{1}{\sqrt{L_1 C_{eq}}} \tag{4}$$

Based on the designed power rating of the bidirectional converter and the charge transfer, the inductor L_1 can be given as

$$L_1 = \frac{1}{C_{eq}}\left[\frac{QnV_L}{2\pi P_{rate}}\right]^2 \tag{5}$$

where P_{rate} is the rating power of the converter and Q is the amount of charge during charging in parallel. The value of inductor L_2 depends on the peak-to-peak of output current ΔI_{L2} and can be expressed as

$$L_2 = \left[\frac{nV_L T_S}{\Delta I_{L2}}\right]^2 \tag{6}$$

The determination of the capacitance value C_{eq}, is based on the capacitor voltage ripple and the amount of charge in the cycle.

$$C_{eq} = \frac{Q}{\Delta V C} \tag{7}$$

The value of high side-voltage capacitor C_H depends on the relationship between the amount of charge to output converter voltage V_2 at the half period (T_S /2) and the voltage ripple on the capacitor C_H. Hence

$$C_H = \frac{(P_{rate}/V_2)(T_S/2)}{2\pi\Delta V C_H} \tag{8}$$

Similarly, the value of low side-voltage capacitor C_L can be expressed as

$$C_L = \frac{(P_{rate}/V_1)(T_S/2)}{2\pi\Delta V C_L} \tag{9}$$

5 Simulation studies

The location of the converter studied here is shown within the blue star in Fig. 8. The total power is 50 MW, and the voltages are 6 and 30 kV. The wind farm cluster is formed by two parallel lines of wind turbines, each containing five wind turbines in series. Hence, there is a total of 10 wind turbines; each rated at 5 MW, 1.2 kV [13–15]. The DC–DC Converter is required to transfer the power in both directions and is connected to the collection bus tie interconnect at the 6 kV side to the 30 kV side. The forward and reverse powers are 50 and 5 MW. Using the equations derived in Section 4, the parameters of the DC–DC converter used for the simulation were calculated and are listed in Table 1.

As the interest is on the converter operation, the system shown in Fig. 8 was reduced to the circuit shown in Fig. 9. The two systems on either side of the converter are represented by two voltage sources behind equivalent resistances and inductances. In practice, the power flow is controlled by the VSC at the onshore substation. However, for the simulation, the power flow was

Table 1 Converter Parameters used for circuit simulation

Parameters		value	
number of modules		5	
low voltage	V_L	6	kV
high voltage	V_H	30	kV
inductor	L_1	2.53	μH
inductor	L_2	110	μH
capacitor in the middle circuit Cn		694.5	μF
capacitor	C_L	83	μF
capacitor	C_H	116	μF
rated power	P_{rate}	+ 50, −5	MW
frequency	F_S	2	kHz

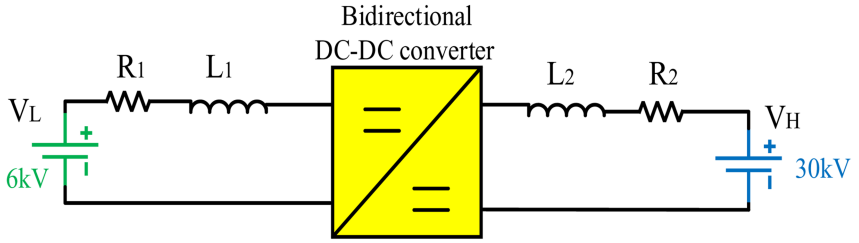

Fig. 9 *Simulation circuit diagram*

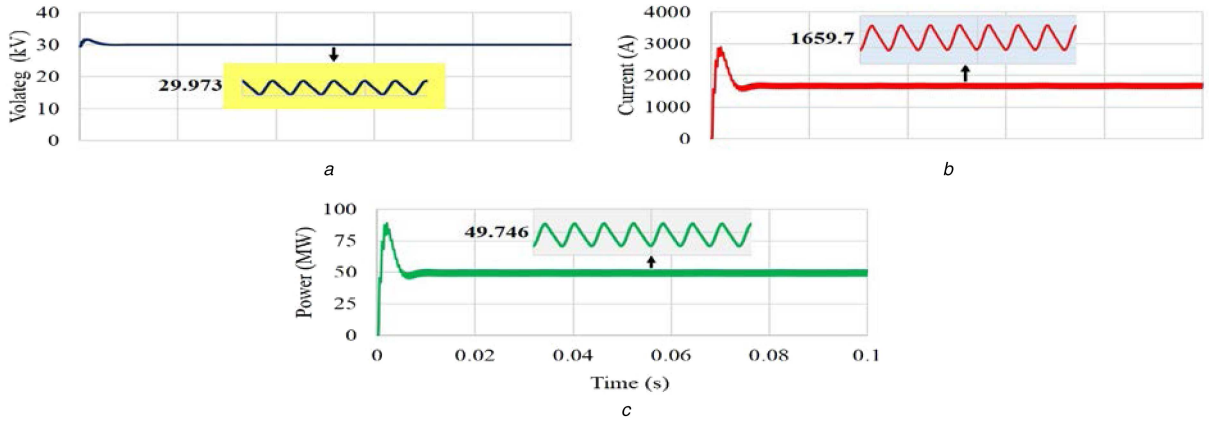

Fig. 10 *Simulation waveforms of the forward mode operation*
(a) Load voltage, ***(b)*** Load current, ***(c)*** Load power

controlled by varying the resistance values R_1 and R_2 on both sides.

The switching frequency F_S of the converter is determined by the LC resonances in the circuit and is 2 kHz, and the fixed duty cycle of $d = 50\%$ was used. The converter is simulated in Matlab/Simulink, using the SimPowerSystem toolbox. The waveforms of the voltage, current, and power during forward mode are depicted in Fig. 10.

The DC gain obtained by the simulation is 4.9, which is very close to the design value of 5. The output voltage, current, and power of the converter in forward mode operation should be 30 KV/ 1667 A, 50 MW as designed. However, the output voltage of the proposed converter is 29.97 KV and the current is 1659 A. In addition, the load power is 49.7 MW as shown in Fig. 10.

As illustrated in Figs. 11*a* and *b*, IGBT and diode currents in modules 1, 2, 3, 4, 5 increases, peaking at 18.6 kA in 250 μs in the last module. IGBTs capable of this duty are commercially available. An example is the IGBT 5SNA 1200G450300 [16].

During discharging the capacitors in series, the voltage across the IGBT switches SC is 6 kV as shown in Fig. 11*c*. However, the voltages across switches S_B increase by 6 kV from left to right reaching a maximum of 24 kV on the shunt IGBT switch at the HV side as shown in Fig. 11*d*. This means that the devices in each module sees different voltages causing manufacturing issues and requiring series connection of devices. In addition, a reverse voltage of 6 kV appears across switches SA as illustrated in Fig. 11*e*.

Waveforms of voltage, current, and power during reverse mode are shown in Fig. 12. The voltage gain obtained by the simulation (0.204) is very close to the theoretical value of 0.2. The output voltage, current, and power of converter in reverse mode operation is also close to the theoretical values.

As illustrated in Fig. 13*b*, the voltage stress on the switch S_b is 6 kV during discharge in series is equal to the $V_H/5$. The charging current in series is the same as through the IGBT switches (ISc = 536 A) as shown in Fig. 13*c*. One can see that the voltage on switches S_b sequentially decreases in 6 kV steps as illustrated in Fig. 13*d*.

6 Conclusions

A new bidirectional DC–DC Marx converter is presented here. Full mathematical analysis led to the design methodology to determine the component values and ratings including solid-state devices. The mathematical equations are validated by simulation. The simulation demonstrated the ability of the converter to interface a 6 kV system with a 30 kV system leading to a gain of 5. The gain can be increased for application to higher voltages by increasing the number of modules. Therefore, the converter is easily scaled up or down. The resonances between the inductors and capacitors are

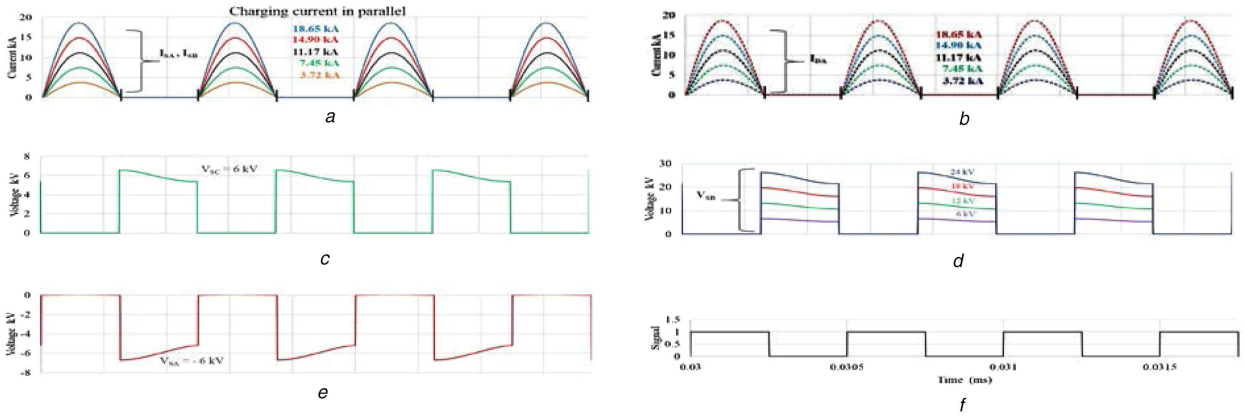

Fig. 11 *IGBT and diode switch simulation waveforms of forward mode operation*
(a) Charging current through IGBTs, ***(b)*** Charging current through diodes, ***(c)*** Voltage across cells C, ***(d)*** Voltage across cells B, ***(e)*** Voltage across cells A, and ***(f)*** Switching pattern

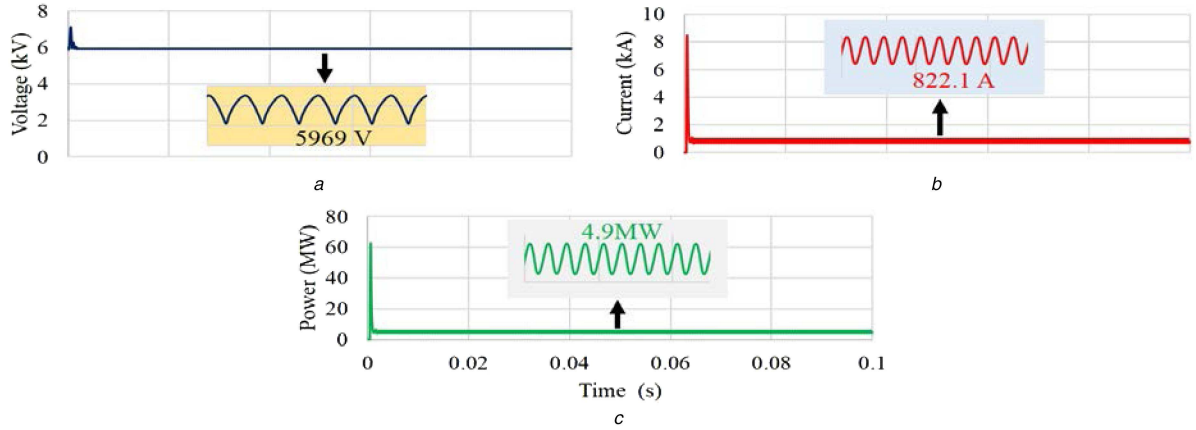

Fig. 12 *Simulation waveforms of the forward mode operation*
(a) Load voltage, ***(b)*** Load current, ***(c)*** Load power

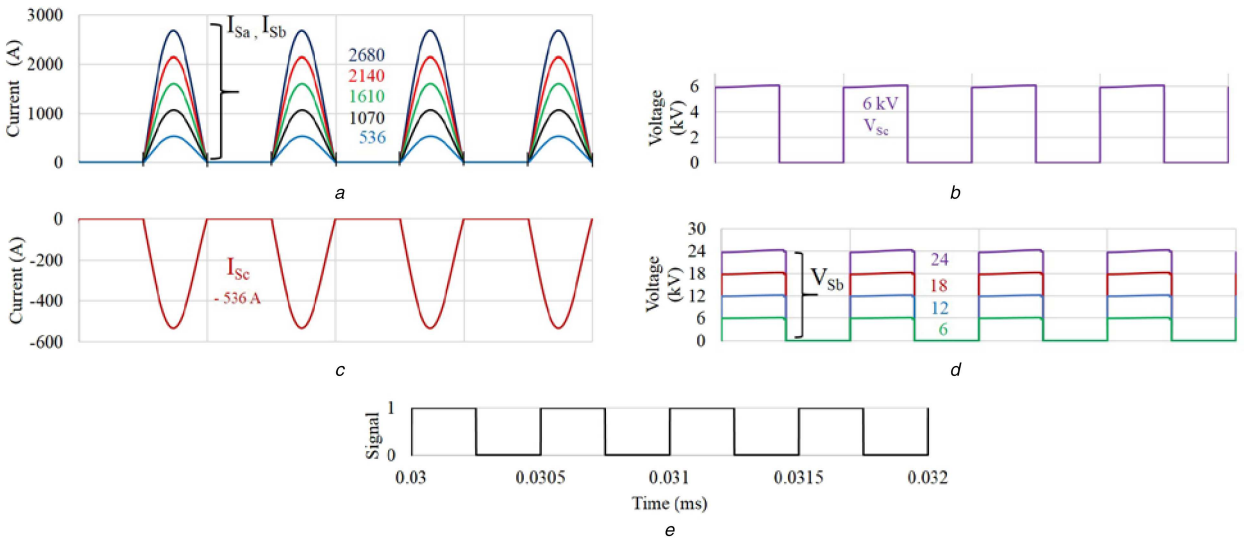

Fig. 13 *IGBT and diode switches simulation waveforms of reverse mode operation*
(a) Currents through cells A and B, ***(b)*** Stress voltage on cells C, ***(c)*** Charging current in series in cells A, and ***(d)*** Step voltage on cells B

used to determine the switching frequency enabling soft switching to reduce the losses.

7 Acknowledgments

The authors would like to thank the Higher Institute of Science and Technology, Alkhums, Libya, and Staffordshire University, Staffordshire, United Kingdom, for funding Mr Samir Milad Alagab PhD.

8 References

[1] Alagab, S.M., Tennakoon, S., Gould, C.: 'Review of wind farm power collection schemes'. 50th Int. Universities Power Engineering Conf. (UPEC), Stoke-on-Trent, UK, 2015, pp. 1–5

[2] Carrizosa, M.J., Benchaib, A., Alou, P., *et al.*: 'DC transformer for DC/DC connection in HVDC network'. 2013 15th European Conf. on Power Electronics and Applications (EPE 2013), Lille, France, 2013

[3] Qin, Z., Shen, Y., Loh, P.C., *et al.*: 'A dual active bridge converter with an extended high-efficiency range by DC blocking capacitor voltage control', *IEEE Trans. Power Electron.*, 2017, **8993**, (c), pp. 1–16

[4] Todor, T., Bauer, P., Ferreira, J.A.: 'Bidirectional modular multilevel DC-DC converter control and efficiency improvements through separate module control method', 2013, pp. 2038–2043

[5] Lagier, T., Ladoux, P.: 'A comparison of insulated DC-DC converters for HVDC off-shore wind farms'. 5th Int. Conf. on Clean Electrical Power Renew. Energy Resour. Impact (ICCEP 2015), Taormina, Italy, 2015, pp. 33–39

[6] Xing, Z., Ruan, X., Xie, H., *et al.*: 'A modular bidirectional buck/boost dc/dc converter suitable for interconnecting HVDC grids'. 2016 IEEE 8th Int. Power Electronics and Motion Control Conf. (IPEMC- ECCE Asia 2016), Hefei, China, 2016, pp. 3348–3354

[7] Pires Fernao, C.A., Foito, D.: 'Bidirectional boost/buck quadratic converter for distributed generation systems with electrochemical storage system'. 5th IET Int. Conf. on Renewable Energy Research and Applications (ICRERA 2016), 2016, vol. 5, pp. 5–10

[8] Jovcic, D.: 'Bidirectional, high-power DC transformer', *IEEE Trans. Power Deliv.*, 2009, **24**, (4), pp. 2276–2283

[9] Jovcic, D., Member, S., Zhang, L., *et al.*: 'LCL DC / DC converter for DC grids', *IEEE Trans. Power Delivery*, 2013, **28**, (4), pp. 2071–2079

[10] Jahromi, M.G., Mirzaeva, G.: 'Design of a high power low losses DC-DC converter for mining applications', 2016, pp. 1–8

[11] Kolparambath, S.K., Suul, J.A.: 'Analysis of DC/DC converters in multiterminal HVDC systems for large offshore wind farms'. Power Energy (TAP), Kollam, India, 2015, pp. 415–420

[12] Filsoof, K., Lehn, P.W.: 'A bidirectional modular multilevel DC-DC converter of triangular structure', *IEEE Trans. Power Electron.*, 2015, **30**, (1), pp. 54–64

[13] Lakshmanan, P., Liang, J., Jenkins, N.: 'Assessment of collection systems for HVDC connected offshore wind farms', *Electr. Power Syst. Res.*, 2015, **129**, pp. 75–82

[14] Alagab, S.M., Tennakoon, S.B., Gould, C.A.: 'A compact DC-DC converter for offshore wind farm application', *Renew. Energy Power Qual. J.*, 2017, **1**, (15), pp. 529–533

[15] Alagab, S.M., Tennakoon, S.B., Gould, C.A.: 'High voltage cascaded step-Up DC-DC marx converter for offshore wind energy systems'. EPE 2017 - assigned jointly to Eur. Power Electron. Drives Assoc. Inst. Electr. Electron. Eng., no. Mmc, 2017, pp. 1–10

[16] ABB Switzerland Ltd.: 'Surge currents for IGBT diodes, application note 5SYA 2058-02', 2014